Solid Freeform Fabrication 2017: Proceedings of the 28th Annual International Solid Freeform Fabrication Symposium – An Additive Manufacturing Conference
Reviewed Paper

316L POWDER REUSE FOR METAL ADDITIVE MANUFACTURING

B. Sartin*, T. Pond*, B. Griffith*, W. Everhart*, L. Elder*, E. Wenski*, C. Cook*,
D. Wieliczka*, W. King†, A. Rubenchik†, S. Wu†, B. Brown*, C. Johnson*, and J. Crow*

*Honeywell Federal Manufacturing and Technology under Contract DE-NA0002839
†Lawrence Livermore National Laboratory under Contract DE-AC52-07NA27344

Abstract

Metal additive manufacturing via laser powder bed fusion is challenged by low powder utilization. The ability to reuse metal powder will improve the process efficiency. 316L powder was reused twelve times during this study, completing thirty-one builds over one year and collecting 380 powder samples. The process, solidified samples, and powder were analyzed to develop an understanding of powder reuse implications. Solidified sample characteristics were affected more by slight process variations than by cycling of the powder. While a small percentage of powder was greatly affected by processing, the bulk powder only observed a slight increase in powder size.

Introduction

The effects on metal powder from processing through laser and electron beam powder bed additive manufacturing (AM) systems are key concerns to industry. An understanding of the implications of powder reuse on the final part characteristics must be developed. This understanding is necessary to ensure component quality while enabling reduction of fabrication costs through powder reuse.

Powder reuse research has been reported by many, especially for Ti64 and nickel alloys [1 - 14]. Typically, these studies found powder particle size to increase [1 - 5] and oxygen levels to rise [4 - 10] with reuse. When mechanical testing was performed, strength increased and elongation reduced in correspondence with the increase in oxygen levels [8, 5]. Limited work has been performed on steels, including 17-4SS [15, 16], 316L [17], and 4340 [18]. Slotwinski et al. found particle size to increase [15] while others documented no consistent trend in size or morphology [16]. Skryecki is the only 316L powder reuse study reviewed, finding only minor variations in particle size and morphology [17]. The reduction in fines in the powder distribution and an increase in larger powder generated through processing were found to improve flowability as determined by various methods [1, 4, 13, 16, 19]. Generally, every finding has a conflicting conclusion in another study, with numerous authors finding no significant changes in the powder or solidified samples. Most authors conclude practical powder reuse may be used with minimal impact on the process results.

In this powder reuse study, a 500kg single lot of 316L stainless steel was processed for twelve reuse cycles. The study was executed over one year, thirty-one builds, and yielded pertinent information on metal AM powder, process, and equipment; and continued to advance the methods for analyzing metal AM powder.

Experimental

Powder used by this study was processed through a Renishaw AM250 laser powder bed AM machine and ancillary sieve according to the process displayed in Figure 1. Powder samples (~500g) are removed at each processing point and solid samples are removed for testing after each build. Powder was processed through each reuse cycle collectively to maintain discrete cycles of powder over the course of multiple builds as presented in Figure 2.

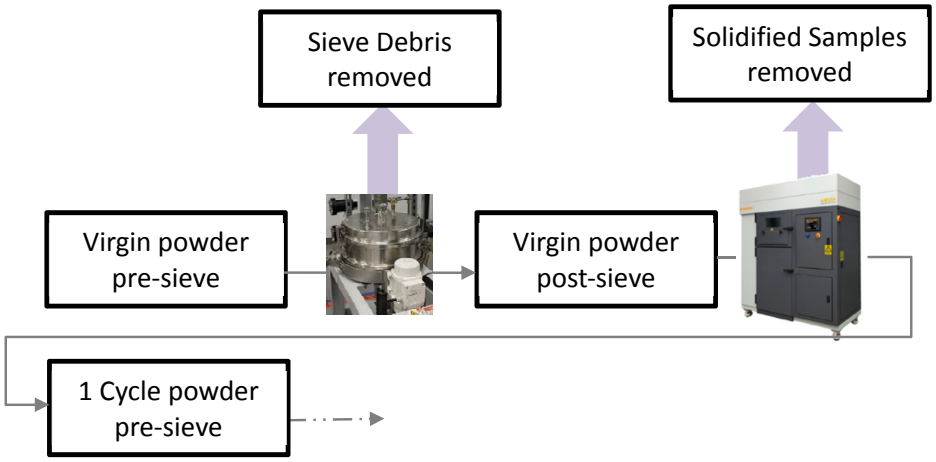

Figure 1: Approach flow chart

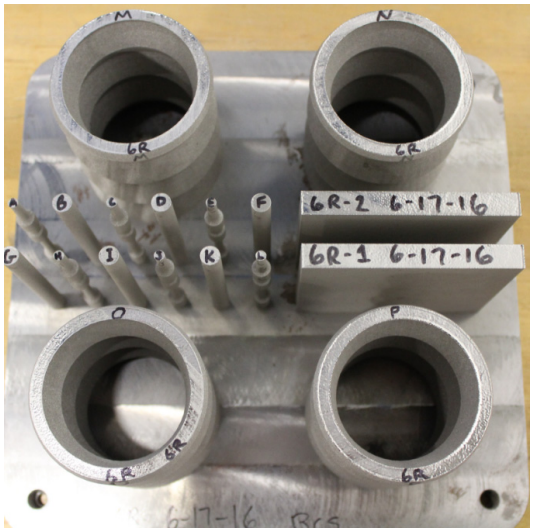

Figure 2: Representative build layout of solidified samples

Build file and parameter definition processing information are presented in Table 1. In addition to these easily controlled inputs, a best effort was made to control other aspects of the process including powder storage along with setup and operation of the equipment (AM machine and sieve). Build anomalies were tracked and powder mass was recorded for each collection point in the process as presented in Figure 3 and Figure 4.

Table 1: Parameter Set Definition

Parameter	Value
Volume (cm^3/cm)	58
Surface Area (cm^2/cm)	189
Laser Time (s/layer)	208

Parameter	Value
Scan Strategy	Meander
P, Hatch Power (W)	200
hs, Hatch Distance (µm)	90
et, Exposure Time (µs)	90
dt, Dwell Time (µs)	10
pd, Point Distance (µm)	50

Parameter	Value
E_p, Point Energy Density (J/mm^2)	4.68
E_L, Linear Energy Density (J/mm^2)	5.14
E_A, Area Energy Density (J/mm^2)	4.00
v_L, Linear Speed (mm/s)	500
v_A, Area Speed (mm^2/s)	49.5

Energy densities and processing speeds noted were calculated as follows:
ss: Laser spot size, diameter (µm)

Point Energy Density (J/mm^2) $$E_p = \frac{P \cdot et}{\frac{\pi}{4} ss^2}$$ Equation 1

Linear Energy Density (J/mm^2) $$E_L = \frac{P \cdot et}{pd \cdot ss}$$ Equation 2

Area Energy Density (J/mm^2) $$E_A = \frac{P \cdot et}{pd \cdot hs}$$ Equation 3

Linear Speed (mm/s) $$v_L = \frac{pd}{et + dt}\left(1000 \frac{\mu m}{mm}\right)$$ Equation 4

Area Speed (mm^2/s) $$v_A = \frac{pd \cdot hs}{et + dt}$$ Equation 5

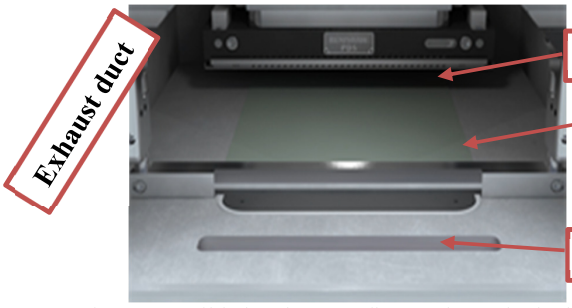

Figure 3: Build chamber overflow and powder bed definition

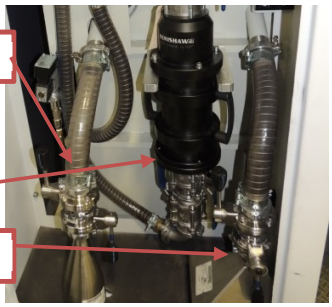
Figure 4: Front/back overflow receivers

Powder was analyzed after various cycles of reuse for composition, size, morphology, skeletal density, moisture, surface characteristics, crystalline structure, laser absorptivity, and flowability. Tests used include but were not limited to combustion or inert gas fusion (LECO), acid digestion followed by iCAP, direct insertion probe mass spectroscopy, ASPEX SEM, Rotap sieving, Helium pycnometry, Karl Fischer titration, vapor sorption, X-ray photoelectron spectroscopy (XPS), scanning electron microscope (SEM) and energy dispersive X-ray spectroscopy (EDS), X-ray diffraction (XRD), calorimetric absorptivity determination [20, 21], powder rheology, Hausner ratio, and Scott volumeter.

Samples fabricated during each build included tensile bars and density pucks. The as-AM tensile test specimens fabricated, corresponding to those used in prior work [22], were similar to that presented in ASTM E8M as subsize R4, with the exception of a 1° gage taper as opposed to a 1% max increase in gage diameter. These samples were produced and tested with an as-AM surface finish. Solidified samples produced from various cycles of reused powder were tested to analyze composition, corrosive properties, crystalline structure, density, porosity, microstructure, mechanical strength and ductility, and surface finish. Tests used include but were not limited to combustion or inert gas fusion (LECO), acid digestion followed by iCAP, copper sulfate testing, XRD, density via Archimedes in alcohol, metallography, Knoop microhardness, tensile testing, SEM fractography, and surface profilometry.

Results and Discussion

Processing

Operating metal AM equipment for an extending period reveals numerous gaps in the current processing equipment and procedures when documented with the rigor associated with this effort. The metal AM equipment used by this study required a significant amount of operator intervention to continue operations as displayed in Figure 6. Despite consistent build geometries, the build duration ranged from 6 to 43 days with an average build duration of 10.4 days ($\sigma = 7.9$). Continued maturation of metal AM equipment will reduce these challenges and allow for more consistent processing.

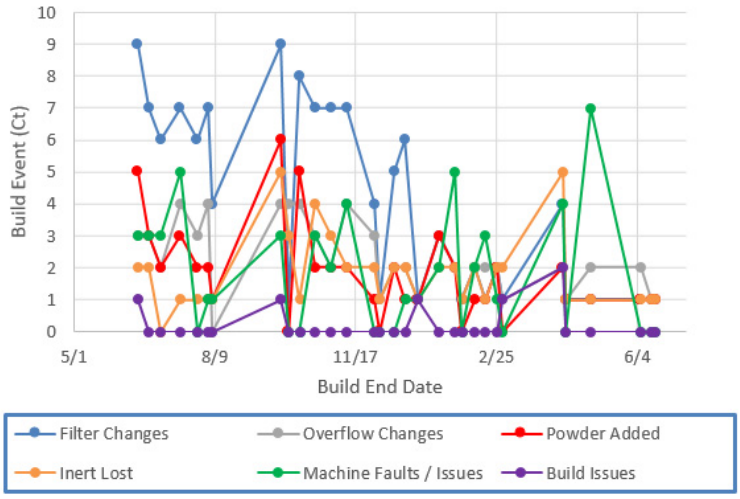

Figure 6: Build event counts

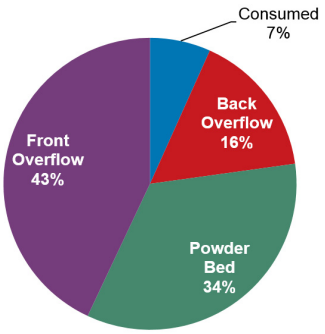

Figure 5: Study mass averages by collection pt

Powder mass values were recorded for all builds to document the percentage of powder associated with each equipment collection location (Figure 3 and Figure 4) and the amount consumed by each processing step. This study found that on average 6.7% of the powder introduced to the system was consumed by the metal AM process when confined to the metal AM equipment, including approximately 2-3% consolidated into the components fabricated, ~1% collected in the AM equipment filtration, and the remainder consumed during the AM equipment and component clean-out process. An additional 3% of the powder was removed during the sieving

process and ~3.5% of the powder was removed as samples to facilitate powder characterization at each cycle of reuse. This process powder utilization of 2-3% aligns with the 3% utilization reported by Hann [10] and the 3 - 6% utilization reported by Kellens et al. [23]

Powder

Inorganic analysis was performed on 228 samples of powder to characterize variation based on collection location and cycle of reuse. No statistical variation was found between collection locations (powder bed, front overflow, back overflow) which will enable reduced sampling going forward. Powder chemistry is affected by the metal AM process; powder collected from the 80µm sieve screen in-between each reuse cycle (debris) tested considerably higher for oxygen and slightly higher for hydrogen (Figure 7). Additionally, the distribution of composition was widened on these samples for oxygen, hydrogen, carbon, sulfur, and titanium. The removal of debris via sieving removed the vast majority of powder that had been chemically altered, however, as there were no statistical trends in the elemental composition observed relative to reuse cycle (Figure 8).

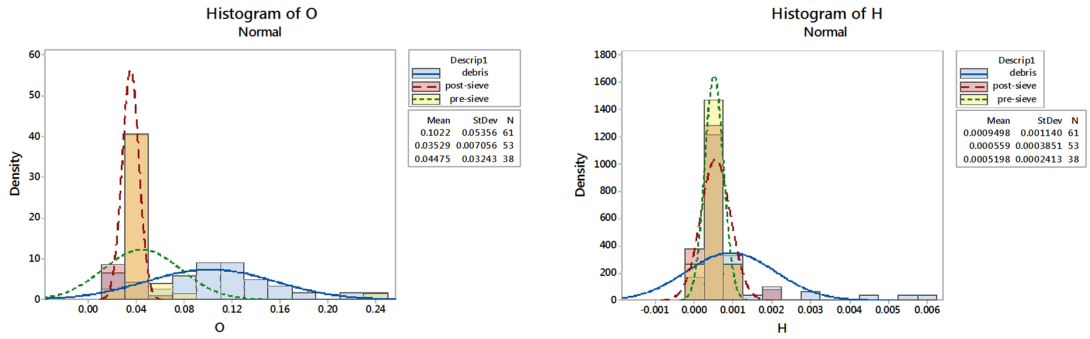

Figure 7: Histograms by processing step, selected test data

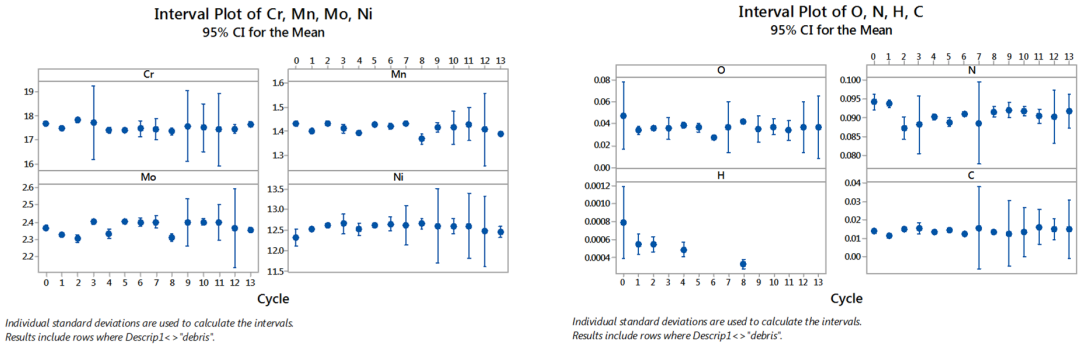

Figure 8: Interval plots of selected elements vs. powder reuse cycle

Organic testing was performed via direct probe mass spectroscopy on a number of articles that comprised the sieving equipment, metal AM equipment, or are otherwise in the process and considered opportunities for contamination. Notable findings include dioctyl phthalate that is free to migrate from the polyvinyl chloride tubing used on the AM equipment and sieving equipment; and acetic acid residue potential from the application of vinegar based Windex™ in the equipment cleaning procedure.

296 powder samples were characterized for size via ASPEX SEM and Rotap sieving. No statistically significant change in size or shape was observable via ASPEX SEM. Particle size distribution as observed via Rotap sieving identified a statistical difference between virgin and eight cycle powder (seven cycles of reuse) with a decrease in the percentage volume of 20 to 25µm powder and an increase in the percentage volume of 45µm and larger powder.

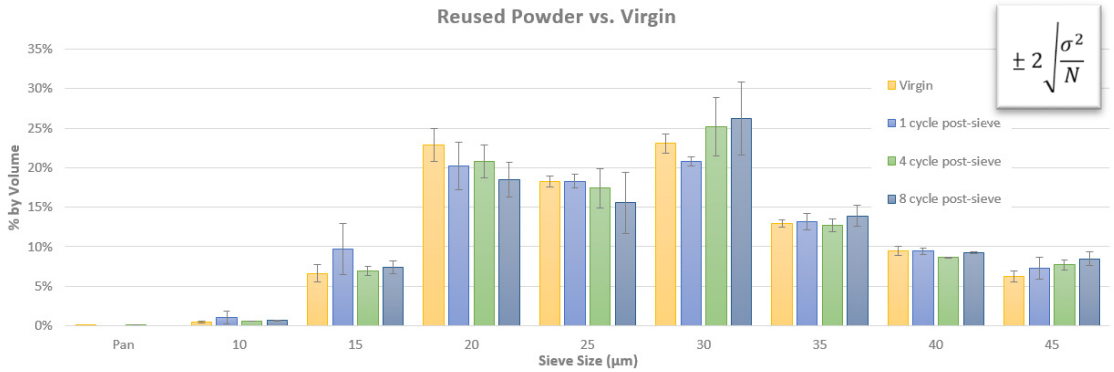

Figure 9: Reused post-sieve powder (combined all collection groups) vs. virgin by cycle

No statistical change was observed for a number of characteristics tested including skeletal density, flowability, and moisture. Skeletal density was performed via Helium pycnometry and remained consistent over eight cycles; measured at 7.957 +/-0.024 g/cc on virgin powder and 7.964 +/-0.030 g/cc on eight cycle powder. Flowability was determined via various methods including Scott's volumeter apparent density and Hausner ratio. The test variability associated with these tests did not allow for differentiation between flowability of various cycles of powder. Moisture was characterized by Karl Fisher titration and vapor sorption. Both methods observed low moisture adsorption in powder, never exceeding 0.0092% by weight.

Flowability testing performed using an MCR302 two vane stirrer at 8 rpm, did differentiate between virgin, four cycle, and eight cycle powder. Three 80 mL samples were tested following air fluidization in the test cell at 1.6L/min. Values reported as cohesion strength were reported as 608, 681, and 771 Pa for the virgin, four cycle, and eight cycle samples, respectively.

Surface characterization was performed on powder after various cycles of reuse via several methods. XPS was used on numerous powder samples with example surveys displayed in Figure 10, where red is as-received, blue is after 720 seconds of 1 kV argon sputter, black is after 2880 seconds of 1 kV argon sputter, and green is all previous exposure plus 30 seconds of 4 kV sputter. During the interrogation of the surface, sputtering reduced Zn to extremely low concentration and Mn was reduced as well. With the removal of these elements along with oxygen, the Cr, Fe, and Ni concentrations increased. The oxygen and carbon are never reduced to zero as the valleys on the surface of the powder particle are not exposed to the argon sputter. Although additional analysis is needed, all three powders analyzed displayed similar signatures regardless of cycle of reuse. The surface of the raw material is rich in Zn and Mn. Compared to a typical bulk stainless steel surface, Fe surface concentration is greater and Cr surface concentration is lower.

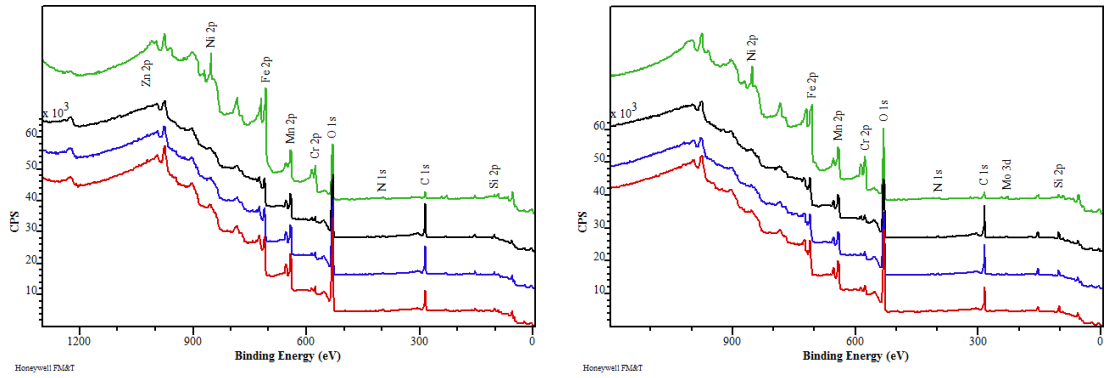

Virgin powder 4 cycle powder, front overflow pre-sieve

Figure 10: XPS surveys for various durations of sputter

SEM was applied to characterize the surface of spatter particles produced by the metal AM process. When material is ejected from the melt pool during active melting, the surface tension yields a spherical particle which, as it solidifies, generates a unique dispersion of elements. Elemental maps and spectrum identified oxide patches on the surface of these particles as silicon oxide (Figure 11 and Figure 12). These finding agree with work performed by Simonelli who noted Mn, Si, and Mg oxides on the surface of laser spatter particles [24].

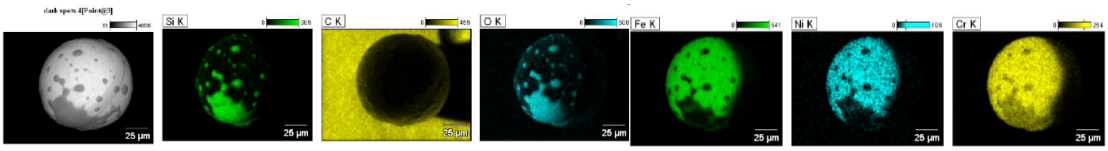

Figure 11: Elemental map of particle

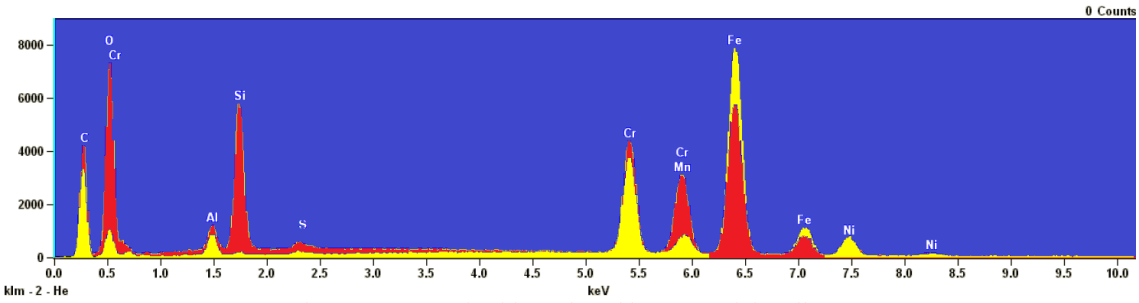

Figure 12: EDS of oxide (red) and base material (yellow)

Absorptivity testing was performed on numerous samples and revealed noticeable differences in absorptivity relative to the sample collection location (Figure 13). A linear fit was applied to the temperature-dependent absorptivity according to Equation 6.

$$A(T) = \alpha + \beta T(°C) \quad \text{Equation 6}$$

where α is the powder absorptivity at room temperature.

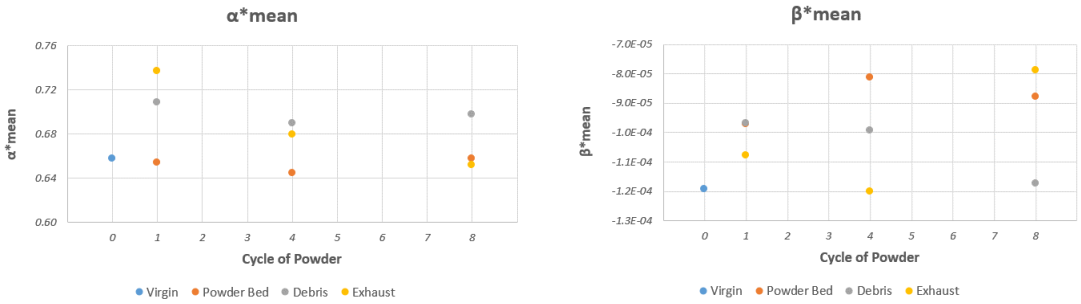

Alpha coefficient Beta coefficient

Figure 13: Absorptivity coefficient scatterplots by collection location and powder cycle

The metal AM process certainly has an impact on the absorptivity of the powder. While there was some variation in the data, material collected from the exhaust duct and from the sieve screen (debris) typically yields higher values for absorptivity. As with particle size and composition, the majority of the material that is altered by the metal AM process is removed via sieving in between each reuse of the powder.

Solidified Samples

Inorganic analysis was performed on 57 solidified samples fabricated as part of this study. There was no consistent statistical trend in composition relative to powder reuse as displayed in Figure 14 for selected elements. Corrosion testing performed via copper sulfate found no indications of free iron on the selected samples.

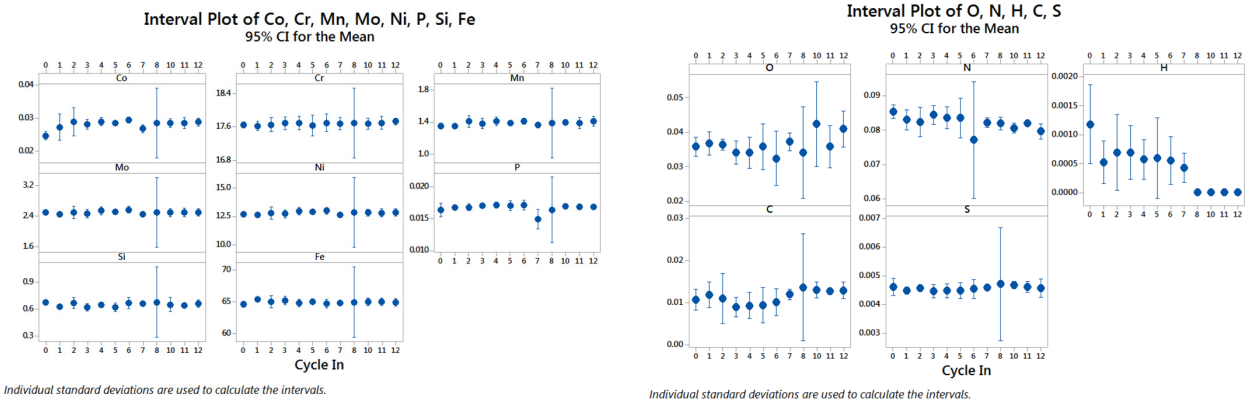

Figure 14: Solid article iCAP chemistry, selected test data

XRD analysis of samples displayed consistent lattice constant (3.615 ± 0.006 Ångström) and unit cell strain is high for metal AM items (0.99 ± 0.06). The lattice constant was consistent with a typical austenitic structure with preferred orientation [25]. XRD revealed two prevalent crystal growth orientations. The preferential crystal growth direction was found to correspond to the (111) Miller index plane followed by the (200) Miller index plane.

Ninety-eight density samples were tested from twenty-eight builds. Density had no consistent trend versus the cycle of reuse, implying that this characteristic is affected by slight variations in the AM process more than the powder reuse cycle.

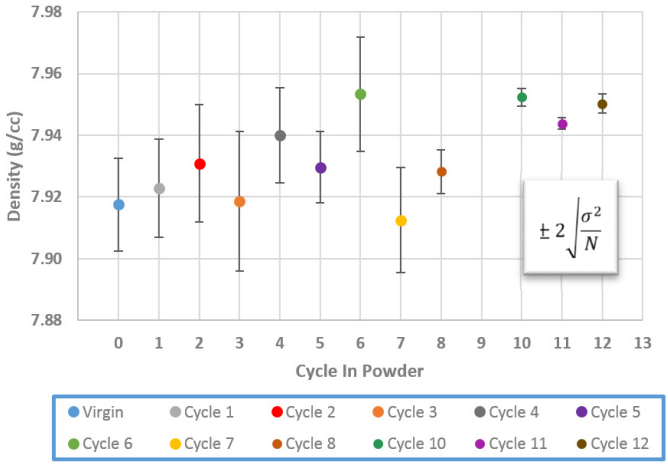

Figure 15: Density values determined via Archimedes in alcohol by powder cycle (average+/- 95% CI)

One hundred eighteen tensile bars were tested in this study. There is no consistent trend in the mechanical strength and ductility relative to powder reuse for up to twelve cycles of reuse. A number of instances of low strength and ductility were observed throughout the study, but these were identified to be caused by various machine or process variations as opposed to being caused by the reuse of powder. The majority of these low strength results are associated with builds in which poor layer fusion was obtained due to either laser muting or laser focus drift. Laser muting is caused by condensate in the build chamber depositing on the lens cover and is compounded by poor gas flow due to filtration restriction. Maintaining laser focal consistency with this equipment was a challenge, and in some instances, despite adequate chamber conditions and focal verification prior builds, was found to be the cause for lack of consolidation.

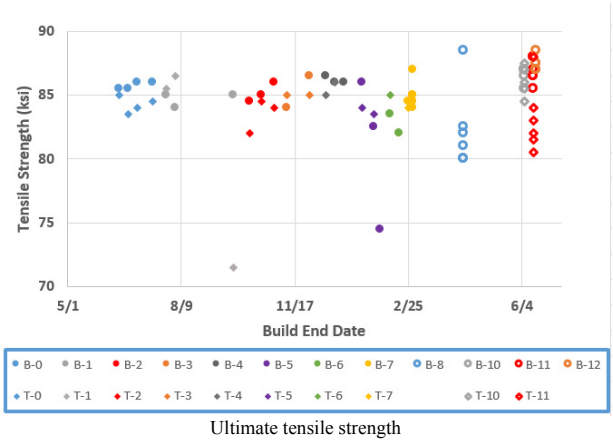

Ultimate tensile strength

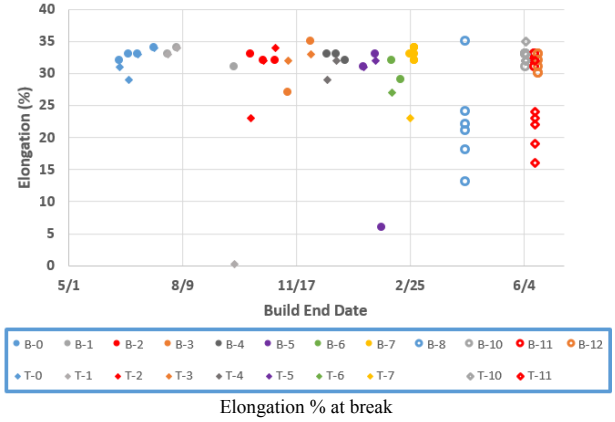

Elongation % at break

Figure 16: As-AM selected tensile results

Review of tensile fractures was performed on a limited number of samples, but provided items for future investigation. A typical fracture is presented in Figure 17 with jagged edges around its circumference. Due to the surface finish of these parts, the failures propagated from numerous locations resulting in a non-uniform macro-cup and cone. Upon close inspection it was determined as ductile fracture due to the observance of microvoids or dimpled structure across the sample. These micro-cup and cone ductile fracture events are observed to be oriented relative to their position on the cross section, with fracture near the center of the sample equiaxed and oriented upwards, slowly changing to shear ductile rupture directionally oriented towards the center of the sample near the extents of the bar.

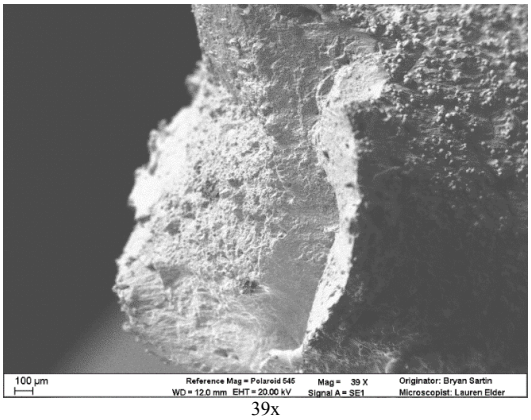

39x

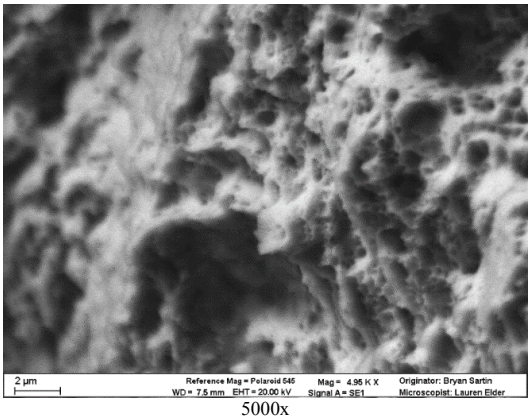

5000x

Figure 17: Typical fracture surface

An example of a non-typical tensile bar fracture that was investigated is presented in Figure 18. Due to poor layer adherence this failure appears to have a majority of cleavage rupture. Lack of solidification was supported by the observance of numerous regions of unmelted powder. Close observance appears to display the upper face of a weld pool, unchanged by the application of subsequent laser passes. This failure was caused by an extended build pause which was not appropriately restarted. During an extended pause, the components being fabricated cool to ambient temperature conditions. Upon restart, the build height is compensated for component thermal shrinkage such that the restarted layer is deposited directly on the last completed layer. This ensures weld penetration into the previously deposited layer, but was not performed according to the standard process in this instance.

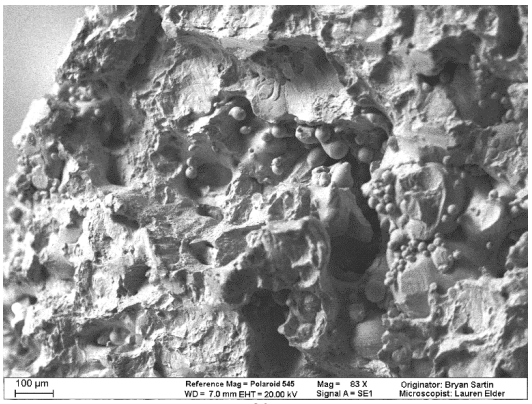

80x

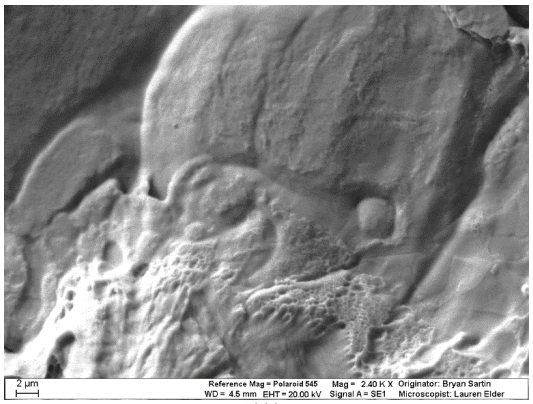

5000x

Figure 18: Cleavage rupture example

One-hundred and fifteen samples were analyzed for microhardness using a 500g Knoop impression. Fifteen to eighteen measurements were taken per sample for a total of 1917 measurements. While there were some localized trends, no consistent statistical trend was observed in microhardness over twelve cycles of powder reuse (Figure 19). Metallography performed in parallel with microhardness observed no consistent trends in sample porosity (maintained below 0.15%) and observed consistent weld penetration depth and melt pool shape (Figure 20).

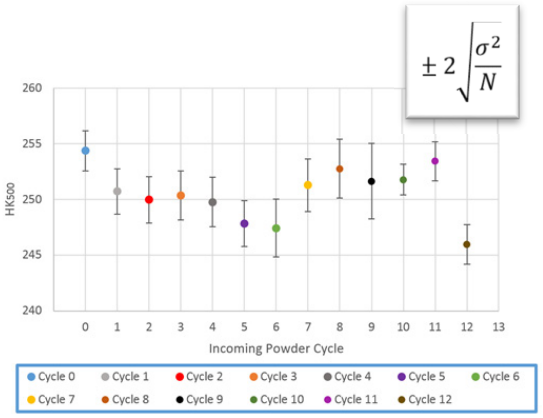

Figure 19: Microhardness data by cycle (ave ± 95% CI)

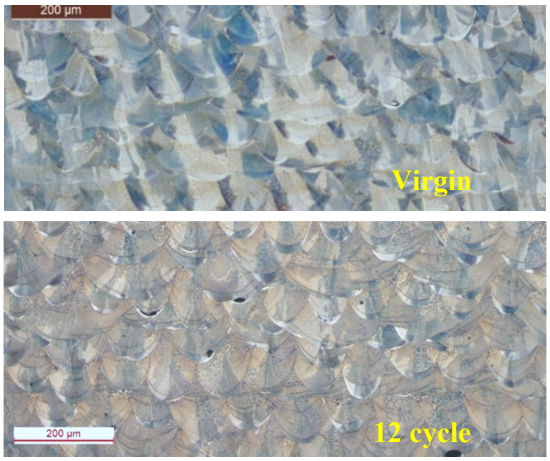

Figure 20: Examples of sample metallography

Surface finish was measured on twenty-two samples with approximately 11 linear inches of readings taken on each sample. Surface finish of items produced was fairly consistent (382.6µin overall mean) regardless of powder cycle as displayed in Figure 21, with some exceptions. Builds occurring with two cycle powder had improved surface finish; attributed to tight gas flow monitoring that occurred over that period. A build using powder that had been reused eight times had poor surface finish; attributed to the metal AM machine becoming inoperable for an extended period of time over the course of that build.

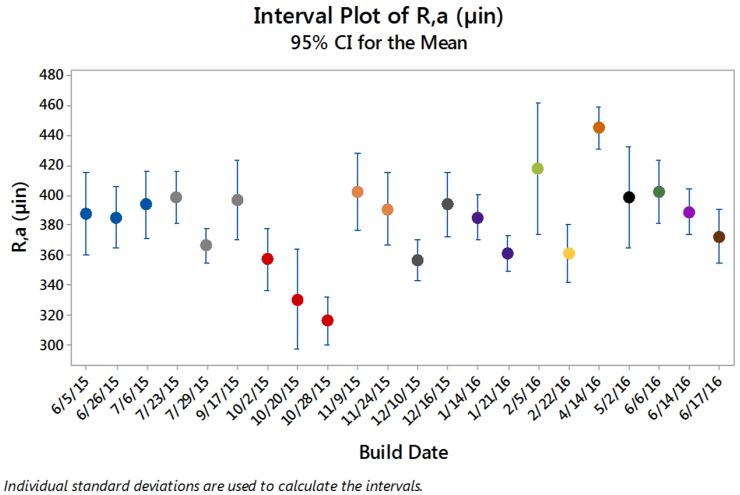

Figure 21: Surface roughness (R,a µin) by build end date

Conclusions and Future Work

For 316L stainless steel, the metal AM process does affect the powder used as observed via Rotap sieving, inorganic, SEM/EDS, and absorptivity testing performed. However, the majority of the powder altered by the process is removed by the sieving process. In this study it was shown that 316L powder may be reused for up to twelve cycles in the laser powder bed fusion process with only minimal statistical variations in the powder size distribution and no consistent statistical variation in the properties reviewed by this study of the components fabricated by the metal AM process.

Powder bed fusion has poor powder utilization at only 2-3%. Additionally, this process is still developing with significant operator intervention required to keep equipment processing and equipment issues resulting in build variation and intermittent equipment down-time. In this study, the process variation associated with this emerging manufacturing technology had a more significant impact on results than did powder reuse.

Future work should be focused on maturation of the metal AM process, reducing operator interaction and improving consistency of critical metal AM equipment settings such as laser energy density, gas flow, and powder layer thickness. Additionally, efforts should include continued development of current powder and solid article analysis methods and the exploration of new methods to ensure repeatable results with suitable sensitivity relative to powder reuse.

Acknowledgements

The authors wish to acknowledge the support of numerous individuals in executing this work including Joseph Goedecke, Ida Sanchez, Joseph Hesting, Joe Morton, Joseph Vellella, Kevin Davis, Rella Greufe, Ann Choi, Emily Webster, Danielle Moore, David Smith, Ben Peterson, Mary Ann Godwin, Nathan Wyeth, Shawn Van Slyke, Ron Koch, Anthony Loveland, Gerald Woodburn, Brandon Volmerding, Justin Tannehill, Jason Gibbs, Jamie Ayers, Diana Goedecke, Jason Rogers, Andrew Cox, Gregory Hawkins, Michelle Maurer, Mary Urrutia, Bradley Teeter, Mark Sourek, Darryl Engelhardt, Michael Sutherlin, Paul Catlett, Karalyn Gibbs, Carol Lusby, Tamera Green, Joel Corkill, Jim Reilly, Michael Gatts, Karl Arnold, Phong Du, Otis Walton, Kaitlin Gill, and Kristen Roy.

This work was funded and performed by Honeywell Federal Manufacturing and Technology under Contract DE-NA0002839 and Lawrence Livermore National Laboratory under Contract DE-AC52-07NA27344. The United States Government retains and the publisher, by accepting the article for publication, acknowledges that the United States Government retains a nonexclusive, paid up, irrevocable, world-wide license to publish or reproduce the published form of this manuscript, or allow others to do so, for the United States Government purposes.

References

[1] Seyda, V., Kaufmann, N., & Emmelmann, C. (2012). Investigation of aging processes of Ti-6Al-4V powder material in laser melting. Physics Procedia, 39, 425-431.

[2] O'Leary, R., Setchi, R., Prickett, P., Hankins, G., & Jones, N. (2015). An Investigation into the Recyling of Ti-6Al-4V Powder Used Within SLM to Improve Sustainability. Cardiff University, School of Engineering.

[3] Sun, Y.Y., Gulizia, S., Oh, C.H., Doblin, C., Yang, Y.F., Qian, M. 2015, "Manipulation and Characterization of a Novel Titanium Powder Precursor for Additive Manufacturing Applications," Journal of Metals (JOM), 67/3: pp. 564-572.

[4] Grainger, L. (2016). Investigating the effects of multiple powder re-use cycles in AM.

[5] Kistler, N. (2017), Characterizing and Managing Metal Powder in AM Service. LPW.

[6] Al-Bermani, S.S., Blackmore, M.L., Zhang, W., and Todd, I., "The Origin of Microstructural Diversity, Texture, and Mechanical Properties in Electron Beam Melted Ti-6Al-4V," Metallurgical and Materials Transactions A (2010) 41: 3422. Doi: 10.1007/s11661-010-0397-x

[7] Grainger, L. (2015). Metal powder reuse in additive manufacturing. Renishaw PLM.

[8] Tang, H. P., Qian, M., Liu, N., Zhang, Z., Yang, G. Y., & Wang, J. (2015). Effect of powder resuse times on additive manufacturing of Ti-6Al-4V by selective electron beam melting. Journal of the Minerals, Metals and Materials Society.

[9] Nandwana, P., Peter, W., Dehoff, R., Lowe, L., Kirka, M., Medina, F., & Babu, S. (2015). Recyclability Study on Inconel 718 and Ti-6Al-4V Powders for Use in Electron Beam Melting. Metallurgical and Materials Transactions.

[10] Hann, B. (2016). Powder Reuse and Its Effects on Laser Based Powder Fusion Additive Manufactured Alloy 718. SAE Int. J. Aerosp., 9(2).

[11] Gaytan, S. M., Murr, L. E., Medina, F., Martinez, E., Lopez, M. I., & Wicker, R. B. (2009). Advanced metal powder based manufacturing of complex components by electron beam melting. Materials Technology, 24(3), 180-190.

[12] Ardila, L., Garciandia, F., Gonzalez-Diaz, J., Alvarez, P., Echeverria, A., Petite, M., . . . Ochoa, J. (2014). Effect of IN718 recycled powder reuse on properties of parts manufactured by means of Selective Laser Melting. Physics Procedia, 56, 99-107.

[13] A. Strondl, O. Lyckfeldt, H. Brodin, and U. Ackelid, "Characterization and Control of Powder Properties for Additive Manufacturing," The Journal of The Minerals, Metals & Materials Society (TMS), Volume 67, Issue 3, pp. 549-554, 2015.

[14] E. Mutchler, A. Carter, “Achieving Process Repeatability,” Stratasys Webinar, May , 2017.

[15] Slotwinski, J. A., Garboczi, E. J., Stutzman, P. E., Feeraris, C. F., Watson, S. S., & Peltz, M. A. (2014). Characterization of metal powders used for additive manufacturing. Journal of Research of the National Institute of Standards and Technology, 119.

[16] Jacob, G., Brown, C., Donmez, A., Watson, St., Slotwinski, J. (2017), Effects of powder recycling on stainless steel powder and built material properties in metal powder bed fusion processes. National Institute of Standards and Technology. https://doi.org/10.6028/NIST.AMS.100-6.

[17] N. Skrynecki, Kundenorienteirte Optimierung des generativen Strahlschmelzprozesses. Aachen: Shaker, 2010.

[18] Jelis, E., Clemente, M. Kerwien, S., Ravindra, N.M., Hespos, M.R.; 2015, “Metallurgical and Mechanical Evaluation of 4340 Steel Produced by Direct Metal Laser Sintering,” The Journal of the Minerals, Metals and Materials Society, Volume 67, Issue 3, pp. 582-589.

[19] Claus Aumund-Kopp, Daniela Zibelius, Juan Isaza, Markus Uhlirsch, “Practical Powder Analysis for Metal Powder Bed Based AM,” Fraunhofer Direct Digital Manufacturing Conference. 2016

[20] Rubenchik, A., Wu, S., Kanz, V., LeBlanc, M., Lowdermilk, W., Rotter, M., & Stanley, J. (2014). Temperature-dependent 780-nm laser absorption by engineering grade aluminum, titanium, and steel alloy surfaces. Optical Engineering, 53(12).

[21] Rubenchik, A., Wu, S., Mitchell, S., Golosker, I., LeBlanc, M., & Peterson, N. (2015). Direct measurements of temperature-dependent laser absorptivity of metal powder. Applied Optics, 54(24), 7230-7233.

[22] Everhart, W., Sawyer, E., Neidt, T., Dinardo, J., & Brown, B. (2016). The effect of surface finish on tensile behavior of additively manufactured tensile bars. J Mater Sci, 3836-3845.

[23] Kellens, K., Evren, Y., Dewulf, W., Duflou, J.R., Environmental Assessment of Selective Laser Melting and Selective Laser Sintering. K.U. Leuven

[24] Simonelli, M., Tuck, C., Aboulkhair, N., Maskery, I., Ashcroft, I., Wildman, R., & Hague, R. (2015). A Study on the Laser Spatter and the Oxidation Reactions During Selective Laser Melting of 316L Stainless Steel, Al-Si10-Mg, and Ti-6Al-4V. Metallurgical and Materials Transactions A.

[25] Dyson, D. J., & Holmes, B. (1970). Journal of the Iron and Steel Institute(208), 469-474.